Microsystem Technologies
https://doi.org/10.1007/s00542-023-05602-x

TECHNICAL PAPER

# An intelligent Island detection scheme to enhance grid resilience

Apoorva Shukla[1] · Soham Dutta[2] · Pradip Kumar Sadhu[1] · Bishwajit Dey[3]

Received: 14 March 2023 / Accepted: 22 December 2023
© The Author(s) 2024

**Abstract**
The importance of strengthening grid resilience has grown with the increase in environmental destruction and modern power grid complexity, as a consequence of power outages inflicted by human intrusion and extreme weather events. Micro-grids (MGs) have proven to be a viable alternative in such circumstances. However, these occurrences are highly unpredictable, resulting in unintended islands of MGs with negative consequences. As a response, alerting its distributed generations about unintended island is indeed a crucial issue for enhancing grid resilience with MG. Therefore, it is essential to develop a technique for the efficient and accurate detection of unintended islands. There has been an increase in the use of micro-phasor measurement units (μ-PMUs) in MG. In the perspective of this, using an efficient μ-PMU, the research provides a method for finding unintended islands in a MG. The μ-PMU analyses the solar generator bus voltage and analyzes it with symmetrical components for island identification. This study introduces a μ-PMU based Fortescue-transform and random forest algorithm method for rapid detection of unintended islanding in distribution generation system. The approach monitors voltage phasor of zero and negative sequence, calculating angular sum over time to distinguish islanding event from other disturbance. Using Matlab/Simulink, the proposed method is evaluated on the IEEE-34 node distribution network. Multiple simulations provide validation for the method's resilient performance. The methodology proposed has a detection time of 20 ms.

## 1 Introduction

Resilience comes from the Latin verb "resilire," meaning "to rebound or recoil." Consequently, resilience in a power system could be described as the capacity to adequately plan, retort promptly, and retrieve rapidly in the event of a power outages caused by a severe unexpected incident (Liu 2015). These severe events are not limited to natural hazards (such as tsunamis, earthquakes, etc.), but it also includes man-made disasters (for instance operator inaccuracy, cyberattack, etc.)(Wang et al. 2015). During these incidents, the performance of the power system degrades in a cumulative manner. The disruptions created by these events differ from those caused by conventional contingencies. The following are the features of these disruptions: (Farzin et al. 2016; Chen et al. 2017):

I. It can affect any component, making the repair and restoration procedure difficult and time-consuming.
II. It can spread rapidly and make a huge portion of the grid powerless.
III. Its forecast, endurance, and range are utterly unclear.
IV. Other crucial elements, such as the communication channel, may also be compromised.

With rapid change in the climate, a rise in cyber-attacks, and the increasing complexities of the grid, it is anticipated that the number of these interruptions will increase, especially in today's distribution system. On the other side, as modern customers' dependency on electricity has increased, and their desire for a constant supply of electricity has prompted development into improving grid resilience.

### 1.1 Motivation

The advancement of micro-grids (MGs) has improved grid resilience i.e. grid operational capabilities amid extreme

✉ Soham Dutta
soham.dutta@manipal.edu

[1] Department of Electrical Engineering, Indian Institute of Technology (Indian School of Mines), Dhanbad 826004, Jharkhand, India

[2] Department of Electrical and Electronics Engineering, Manipal Institute of Technology, Manipal Academy of Higher Education, Manipal 576104, Karnataka, India

[3] Department of Electrical Engineering, Adani University, Ahmedabad 382421, Gujarat, India

Published online: 30 January 2024

weather events, especially when it comes to continual power delivery to loads which are critical such as hospitals, data centers, etc. A micro-grid is a grid unit spanning a smaller area which has its own power and load requirements. It has the ability to operate independently or in conjunction with the grid (Dutta et al. 2023). Under extreme weather conditions, the generation, storage of electrical power and control becomes difficult within the islanded MG. A proper islanding plan may make the occurrences less severe, allowing for a more rapid and effective reaction. A system that is not connected to the main power grid but energized by distributed generators (DGs) is referred as an island system (Dutta et al. 2022). In order to avoid blackouts, maintenance, etc., intentional islanding is performed with the permission of the power grid controller. In contrast to intentional islanding, unintended islanding arises throughout extreme events without prior knowledge of the operator, trying to pose implications in the islanded zone, such as inconvenience in the coordinated revival of power supply, power quality deterioration because of severe fluctuations in frequency and voltage, and life-danger to the workers involved in maintenance who are uninformed that segregated lines are still energized by DG (Verma et al. 2019). The disconnected but electrified cables can also be hazardous to the people, especially during the event of floods in which individuals may get electrocuted brutally. Hence, real-time awareness and presentation strategies for unintended islanding in distribution generation is necessary (Mumtaz et al. 2023). Because of lacking situational-awareness, the repair process is also delayed after the extreme conditions. Therefore, it is necessary to alert DG about the islanding situation as soon as feasible so that appropriate management measures can be done to ensure the safe continuation of power in MG. Consequently, unintended islanding identification is the initial step in constructing a robust MG. Phasor measurement units (PMUs) are already prevalent as effective instruments for transmission system monitoring. Micro phasor measurement unit (μ-PMU) have also begun to establish themselves in the distribution grid. As μ-PMU has a high sample rate and excellent precision, they may be used to detect unintended islanding in MG.

### 1.2 Literature review

There is a vast variety of islanding recognition approaches that can be found in the academic data. These methods can be arranged into the broad areas of hybrid, signal processing, passive, active, local, and intelligent classifiers (Manikonda and Gaonkar 2019; Dutta et al. 2018a; Mohanty et al. 2023; Shukla et al. 2023).

When using passive sensors, islanding can be identified while a specific aspect of a captured signal achieves a number that is greater than a threshold that has been previously established. Most common passive islanding sensing methods include rate of change of frequency, inverter non-linear approach, harmonic distortion, rate of change of power, phase jump detection, and under/over voltage or frequency (Freitas et al. 2005). The modal component (Makwana and Bhalja 2017), optimized voltage shift (Liu et al. 2016), the inverse hyperbolic secant function, the intrinsic time decomposition (Nale et al. 2019), and the active rate of change of frequency relay (Gupta et al. 2016) are all recent passive approaches. Active sensors are able to overcome the drawback of having a high non-detection zone (NDZ) that is present in the majority of passive approaches. In active sensors, some disturbances are purposefully infused into the grid, and the effect of this is detected through various signals. The most common active sensing techniques include active frequency drift, slip mode frequency shift, Sandia voltage shift, Sandia frequency shift, negative phase sequence current injection, and frequency locked loop-based frequency positive feedback (Ropp et al. 1999; Liu et al. 2010; Trujillo et al. 2010; Lopes and sun 2006; Karimi et al. 2008; Barkat et al. 2023). The power quality of the system is severely degraded when active schemes are used because active schemes inject disturbances into the system.

In order to eliminate the limitations of both passive as well as active detection systems, hybrid sensors combine the two sensing techniques into a single technology. The power line carrier communication, transfer trip scheme and variational mode decomposition are examples of notable local islanding sensing approaches (Reddy et al. 2023; Thakur et al. 2023). The schemes make use of the communication channels that exist between distributed generators and control centres in order to detect island scenarios. These methods do not have any NDZ but come at an extremely high cost. Researchers have found that using sensing methods that involve signal processing has helped them overcome the limitations of the aforementioned sensing methods. In signal processing approaches, relevant signals are evaluated by tools such as wavelet transform, Stockwell transform, hybrid Stockwell transform, Hilbert Huang transform, time-time transform, and mathematical morphology (Do et al. 2015; Niaki and Afsharnia 2014; Raza et al. 2015) for islanding identification in order to extract hidden information. These tools are used to uncover hidden information.

In almost all of the sensing approaches, determining an acceptable threshold value to use in recognising islanding signals is a laborious operation that needs to be accomplished. The problem of determining an appropriate threshold value can be effectively solved by the appropriate training of intelligent classifiers. Effective islanding detection makes use of intelligent classifiers like fuzzy

logic, support vector machine, artificial neural network, and decision tree (Fayyad and Osman 2010; Somalwar et al. 2023; Al-Momani et al. 2023; Heidari et al. 2013; Lidula and Rajapakse 2012; Dash et al. 2012; Mohanty et al. 2014). Island identification is accomplished through the application of principal component analysis to wide area phasor measurements in. Using synchrophasor data in real time hardware, three distinct island sensing approaches are used in. In the case of island sensors, a technique known as " PMU continuous sync-check" is utilised (Laverty et al. 2015; Arefin 2024). For identification of island using PMU data, Kumar and Bhowmik (2018) uses the multiplier approach, a method based on Andrews' plot, and an artificial neural network. In (Dutta et al. 2018b; Singh et al. 2021), a Fortescue transform-based micro-PMU is utilised for island sensing.

Estimating phasors requires some time when it comes to methods that make use of PMU. This results in a lag in the island identifying method, that is something which should be avoided under extreme situations. In addition, the PMU approaches are extremely reliant on the communication network, that might become disturbed whenever there is a significant amount of noise or interference in the environment. On the contrary hand, the majority of the approaches that do not utilise PMU require additional arrangements to be made solely for island identification. This results in a significant increase in both the amount of time necessary for implementation and the amount of money spent. The purpose of this work is to offer a new island detection scheme in order to combine the benefits of utilising the software and hardware of μ-PMU while, consequently, reducing the amount of time spent on phasor estimates.

### 1.3 Advantages of the method

μ-PMU, one of the most valuable components of a distribution generation, has demonstrated its value in harmonic projections, fault analysis and prevention, state estimation, dynamic surveillance, etc. The suggested intelligent island detection system takes into account the availability and usage of μ-PMU. It requires the construction of a separate function within the installed μ-PMU. The μ-PMU monitors the voltage signals at a predefined DG site and conducts symmetrical component analysis for island event separation from other events. The following is a summary of the proposed technique's contributions:

I. The communication, hardware, and software components of PMU are leveraged to detect islanding occurrences. Therefore, system workers is capable to re-establish power to the islanded MG in extreme conditions in a quicker manner.
II. When the communication link between the control centre and μ-PMU is interrupted due to harsh situations, this will be of great assistance. This boosts grid resilience even further.
III. This above mentioned technique is quite simple, and has a high detection speed of 20 milliseconds, and zero NDZ.

### 1.4 The structure of the paper

The manuscript is fashioned as stated. Unit 2 delivers detailed information of necessities in the smart μ-PMU. The development of the presented approach is described in Unit 3. The outcome of the approach in various conditions is discussed and validated in Unit 4. In Unit 5, the technique is equated against the existing islanding detection approaches. The method is concluded in the last Unit 6.

## 2 Necessities for the smart μ-PMU

The functional operation of a conventional μ-PMU in a distribution grid is illustrated in Fig. 1, which provides a graphic picture of this process. In a manner analogous to that of the PMU, the μ-PMU obtains current and voltage signals via potential transformer (PT) /current transformer (CT), calculates phasors using a digital signal processing algorithm, time stamps it with time reference as per the global positioning system, and thereafter transmits the information to the control centre (Pal et al. 2017). In order to achieve accurate monitoring in distribution MGs that use μ-PMU, some problems need to be met (Zanjani et al. 2018). Because distribution networks contain higher resistance than reactance, both reactive power flow and the real power flow cannot be segregated. As a result, the conventional estimated power equations cannot be used. The magnitude as well as the phase angle change are typically on the order of $10^{-4}$ per unit and 0.01°, respectively, due to the fact that the variation in power flows and bus distances are much shorter than those that exist in the transmission system. Moreover, a high harmonic content can be found as a result of the numerous power electronic converters that are utilised in the process of integrating energy from renewable sources into to the distribution system. As a result, μ-PMUs have a precise sensor, lower total voltage error, larger sampling rates, and lower phase uncertainties, all of which contribute to high resolution data (Dutta et al. 2020). Because high-resolution data is to be used for any method analysis of signal processing in a shorter amount of time, this benefit of μ-PMU can be availed for island detection.

In addition, the measurability of a transmission system is simple because it includes a smaller quantity of buses, whereas the measurability of the distribution system is

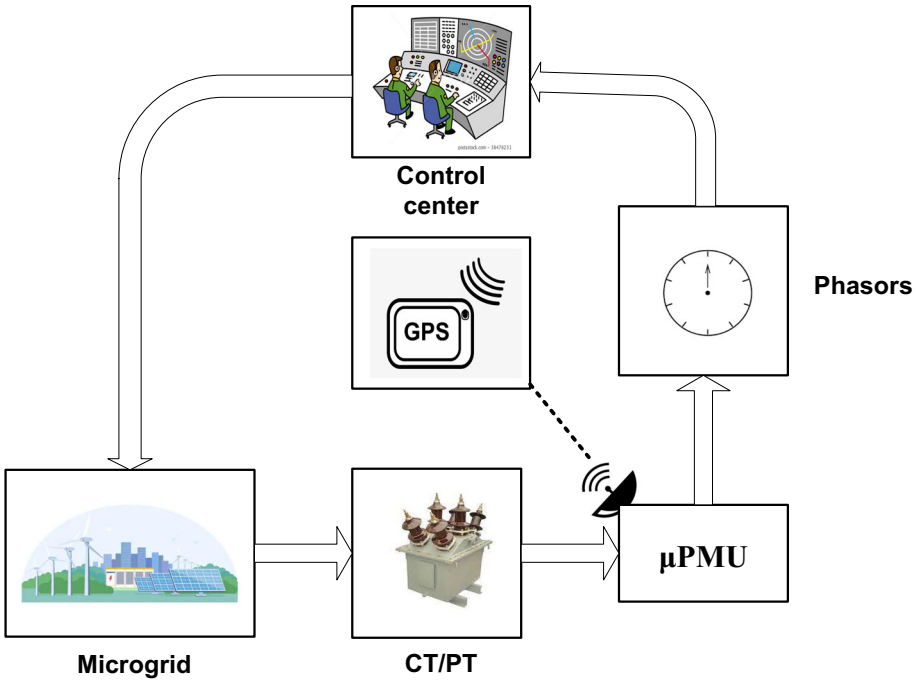


**Fig. 1** Functional operation of a conventional μ-PMU

significantly more difficult since it includes a greater quantity of buses. The changing trend of renewable energy sources is another reason for concern introduced by these sources. As a result, making suitable decisions on control actions can be challenging. Because of this, a more advanced signal analyzer as well as a classifier that is accurate are required. The amount of time needed for recovery after an extreme disturbance is an important consideration. The phasor computation is a time-consuming process. In addition, there is a possibility that the communication link between the μ-PMU and the control centre will become broken when extreme conditions are present. So, in the intelligently updated μ-PMU that has been presented, there is a distinct subroutine that is supplied for island detection in order to cut down on the amount of time needed for detection of island and its dependence upon the communication network. The program directly receives recorded signals through CT/PT and utilises symmetrical component to do analysis on the sampled values while operating inside a window of a predetermined length. A random forest (RF) classifier is given the data that has been processed or extracted so that it can make appropriate event classifications.

## 3 Development of the proposed methodology

Utilizing an enhanced IEEE-34 node distribution test generator in MATLAB/SIMULINK, the approach suggested is validated. In the following sections, the modifications to the traditional IEEE-34 node distribution test generator and the necessary assumptions are described.

### 3.1 Proposed test system

Figure 2 depicts the IEEE 34 node distribution system employed in this paper. The standard frequency is assumed to be 60 Hz. The resistance of the distribution lines is supposed to be R = 0.539 /km and the inductance is expected to be L = 0.4631 H/km (Menon and Nehrir 2007). The IEEE-34 node test feeder network is modified to simulate an islanding scenario. Node 838 is where the local loads are wired into a solar DG that is then connected to the grid. In addition, a μ-PMU is connected to the DG bus. When upstream circuit breakers are opened, islanding is presumed to have occurred. At an irradiation of 1000 W/m2, the solar DG may produce up to 100 KW. The solar DG comprises a 250 kVA, 250 V/25 kV transformer, a 10 kVAR capacitor bank, and a 5 kHz DC to DC boost converter for grid integration. Additionally, the DG has a maximum power point tracking system, a three-phase, three-level inverter featuring pulse width modulation and phase lock loop, and a 10 kVAR capacitor bank.

### 3.2 Fortescue transform

A set of unbalanced '$N_i$' phasors can be transformed into a set of balanced ''$N_i$' phasors, as described by FTT. In FTT, the ''$N_i$' phases determine which transformation matrix is used. The Fortescue matrix equation is provided

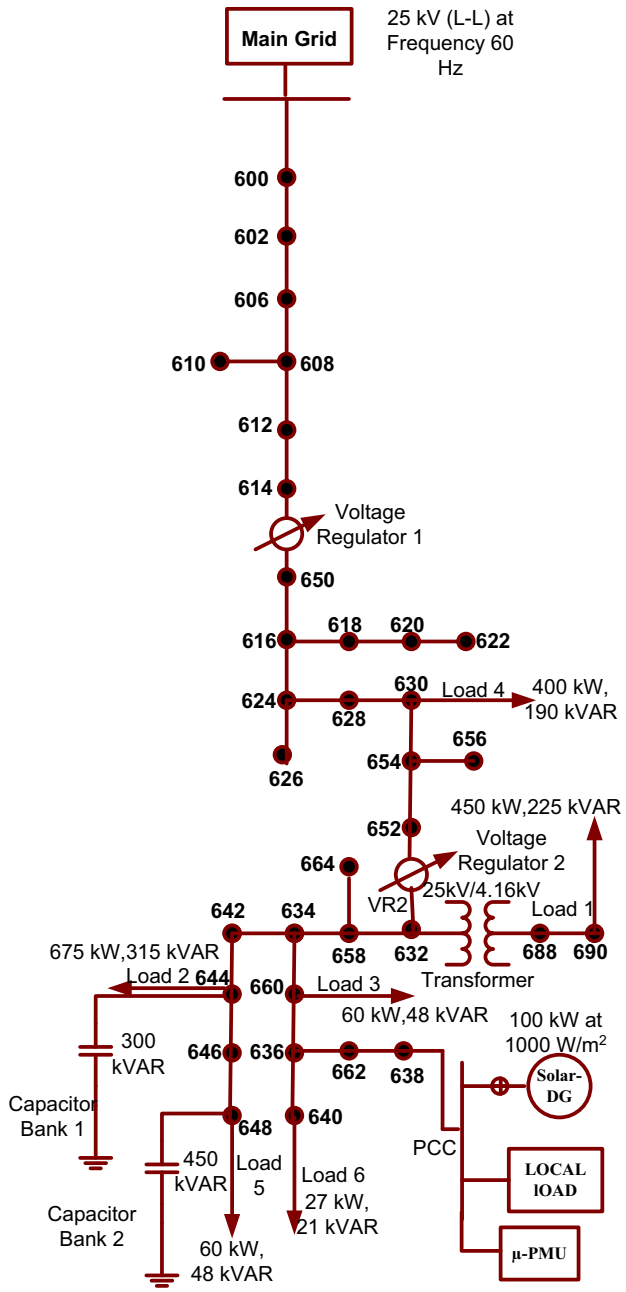


**Fig. 2** Adapted IEEE-34 node system network

by (1), where operator T= $e^{j2\pi/N_i}$ for any $N_i$-phase sequence component. By utilising this operator, one's phase is rotated by $2\pi/N_i$radian. In the case of three-phase power system laterals, $N_i$=3, the three phase voltage phasors ($E_{RYB}$) are represented as the product of three phase positive ($E_{RYB+}$), three phase negative ($E_{RYB}\_$), and three phase zero ($E_{RYB0}$) sequences, respectively, as shown in (2); or, in compressed form, as shown in (3), where $f_T$ represents the Fortescue transformation matrix. The variables $E_{RYB}$ denoted as $E_{RYB+}$, $E_{RYB-}$, and $E_{RYB0}$ each represent a voltage matrix of size 3 × 1 corresponding to a positive, negative, or zero sequence, respectively, of the three voltage phases. The symbol $E_{R\pm0}$ denotes a 3 × 1 matrix consisting of the phase R voltage's positive, negative, and zero sequences. The aforementioned system produces identical magnitudes and phases for both the positive and negative sequence components, with a phase difference of 120°. In contrast, the zero sequence component system exhibits identical magnitudes and phases throughout all phases. The FTT for three phase voltages, expressed in matrix form, is as follows (4) where$E_R$ denotes the magnitude of voltage of phase R, $\angle\beta_R$ denotes the phase angle of voltage phase R,$E_Y$ denotes the magnitude of voltage of phase Y, $\angle\beta_Y$ denotess the phase angle of voltage phase Y, $E_B$ denotess the magnitude of voltage of phase B, $\angle\beta_B$ denotes the phase angle of voltage phase B, $E_{R+}$ denotess the magnitude of positive sequence component of phase R, $\angle\beta_{R+}$ denotes the angle of positive sequence component of phase R,$E_{R-}$ denotes the magnitude of negative sequence component of phase R, $\angle\beta_{R-}$ denotes the angle of negative sequence component of phase R and $E_{R0}$ represents the magnitude of zero sequence component of phase R, $\angle\beta_{R0}$ represents the angle of zero sequence component of phase R.

Consequently, the expanded form and system symmetric component for the phase represented as 'R' in the matrix form are calculated using the Eqs. (5, 6), where $f^{-1}$ represents the inverse FTT matrix. The system sequence components for the remaining phases are assessed in accordance with (7)-(9). In this context, $E_{Y+}$ denotes the positive sequence phasor for phase voltage Y, $E_{Y-}$ signifies the negative sequence phasor for phase voltage Y, $E_{Y0}$ signifies the zero sequence phasor for phase voltage Y, $E_{B+}$ signifies the positive sequence phasor for phase voltage B, $E_{B-}$ signifies the negative sequence phasor for phase voltage B, and $E_{B0}$ signifies the zero sequence phasor for phase voltage B. $E_{R+}$ signifies the positive sequence phasor for phase voltage R. $E_{R-}$ signifies the negative sequence phasor for phase voltage R and $E_{R0}$ signifies zero sequence phasor for phase voltage R.

As demonstrated in (10) and (11), it is possible to deduce that, under balanced system conditions, only positive sequence components will be retained, and their value will be equal to the phase voltage. Consequently, E= $E_{R+}$and β = $\beta_{R+}$hold true for a balanced system. The algorithm under consideration is illustrated in Eq. (12) and utilises the phase angle of the three-phase voltage signal acquired at PCC, which is the angle between the zero and negative sequences. The geometric construction of zero and negative sequence phasors can be used to interpret the proposed method by considering its operator 'T' as a rotational operator of 120°, as illustrated in Fig. 3a and b. Thus, as illustrated in Fig. 3c, angular sum of the zero and

negative sequence phase angles under unbalanced conditions. By establishing this angle addition as a threshold, islanding cases can be identified.

$$\begin{bmatrix} E_0 \\ E_1 \\ E_2 \\ \vdots \\ E_{(N_i-1)} \end{bmatrix} = \frac{1}{N_i} \begin{bmatrix} 1 & 1 & 1 & \dots & 1 \\ 1 & T_{N_i} & T_{N_i}^2 & \dots & T_{N_i}^{(N_i-1)} \\ 1 & T_{N_i}^2 & T_{N_i}^4 & \dots & T_{N_i}^{2(N_i-1)} \\ \vdots & \vdots & \vdots & \vdots & \vdots \\ 1 & T_{N_i}^{(N_i-1)} & T_{N_i}^{2(N_i-1)} & \dots & T_{N_i}^{(N_i-1)(N_i-1)} \end{bmatrix} \begin{bmatrix} E_A \\ E_B \\ E_C \\ \vdots \\ E_{N_i} \end{bmatrix} \tag{1}$$

$$E_{RYB} = E_{RYB+} + E_{RYB-} + E_{RYB0} \tag{2}$$

$$E_{RYB} = F_T E_{R+-0} \tag{3}$$

$$\begin{bmatrix} E_R\angle\beta_R \\ E_Y\angle\beta_Y \\ E_B\angle\beta_B \end{bmatrix} = \begin{bmatrix} 1 & T^2 & T \\ 1 & T & T^2 \\ 1 & 1 & 1 \end{bmatrix} \begin{bmatrix} E_{R+}\angle\beta_{R+} \\ E_{R-}\angle\beta_{R-} \\ E_{R0}\angle\beta_{R0} \end{bmatrix} \tag{4}$$

$$E_{R+0-} = F_T^{-1} E_{RYB} \tag{5}$$

$$\begin{bmatrix} E_{R+}\angle\beta_{R+} \\ E_{R-}\angle\beta_{R-} \\ E_{R0}\angle\beta_{R0} \end{bmatrix} = \frac{1}{3} \begin{bmatrix} 1 & T & T^2 \\ 1 & T^2 & T \\ 1 & 1 & 1 \end{bmatrix} \begin{bmatrix} E_R\angle\beta_R \\ E_Y\angle\beta_Y \\ E_B\angle\beta_B \end{bmatrix} \tag{6}$$

$$E_{Y+} = T^2 E_R, E_Y = T E_{R-} \tag{7}$$

$$E_{YB+} = T E_{R+}, E_{B-} = T^2 E_{R-} \tag{8}$$

$$E_{Y0} = E_{B0} = E_{R0} \tag{9}$$

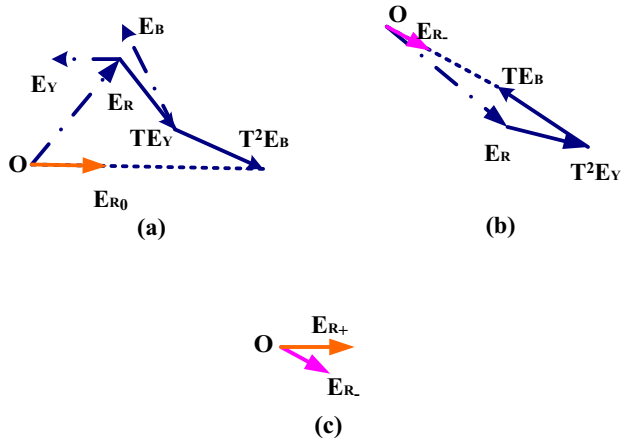


**Fig. 3** Fortescue transform geometric construction of **a** zero sequence **b** negative sequence **c** angular sum of zero and negative sequence phasors

$$\begin{bmatrix} E_{R+}\angle\beta_{R+} \\ E_{R-}\angle\beta_{R-} \\ E_{R0}\angle\beta_{R0} \end{bmatrix} = \frac{1}{3} \begin{bmatrix} 1 & T & T^2 \\ 1 & T^2 & T \\ 1 & 1 & 1 \end{bmatrix} \begin{bmatrix} E_R\angle\beta_R \\ TE_R\angle\beta_R \\ T^2E_R\angle\beta_R \end{bmatrix} = \begin{bmatrix} E_R\angle\beta_R \\ 0 \\ 0 \end{bmatrix} \tag{10}$$

$$E_R\angle\beta = \frac{1}{3}\left(TE_Y\angle\beta_Y + T^2E_B\angle\beta_B + E_R\angle\theta\beta_R\right) = E_{R+}\angle\beta_+ \tag{11}$$

$$\beta = \angle\left[\frac{1}{3}\left(TE_Y\angle\beta_Y + T^2E_B\angle\beta_B - T^2E_Y\angle\beta_Y - TE_B\angle\theta\beta_B\right)\right] \tag{12}$$

### 3.3 Random forest algorithm

Random forest algorithm is an ensemble machine learning procedure that integrates the prediction method. There are two categories of hyper-parameters in random forest algorithm: (1) the count of splits on the subset and (2) the count of trees on the forest (Ashwin et al. 2023). Two challenges are observed in the interim. To determine the finest sequence, the training samples are initially selected at random based on their complexity. The second complexity arises from the absence of clipping energy consumption in this method, which indicates that there is a limit number of trees in each forest. The capacity demand in the proposed method is accurately predicted by the Random Decision Forest (RDF), which is dependent on the historical dataset. Figure 4 illustrates the random forest algorithm structure.

As seen in Fig. 4 and described in detail below, the RF classifier works as follows. Training the RF classifier is covered in stages 1–6, while actual classification occurs in stage 7 (Ashwin et al. 2023).

Stage: 1 Being A = 1 to $C_t$ where, $C_t$ denotes the complete count of trees.

Stage: 2 Under the condition that the number of bootstrap aggregation does not exceed the size of the training sample, generate a bootstrap sample from the training data set.

Stage: 3 Develop a random forest tree $RFT_A(U,E_A)$ based on the bootstrap sample, where U is an input vector and $E_A$ is a random vector with $V_R$ random integers that must be less than or equal to the number of traits in U. First, $V_R$ variables are chosen from a set of traits, and then the best variable is chosen. At this point, the node has split into two child nodes. This process is done again and again until the maximum depth is reached.

Stage: 4 A = A + 1.

Stage: 5 If A$\leq C_t$, go to step 1 if not, go to step 6.

Stage: 6 Get the list of trees as$[RFT_A(U,E_A), A = 1toC_t]$

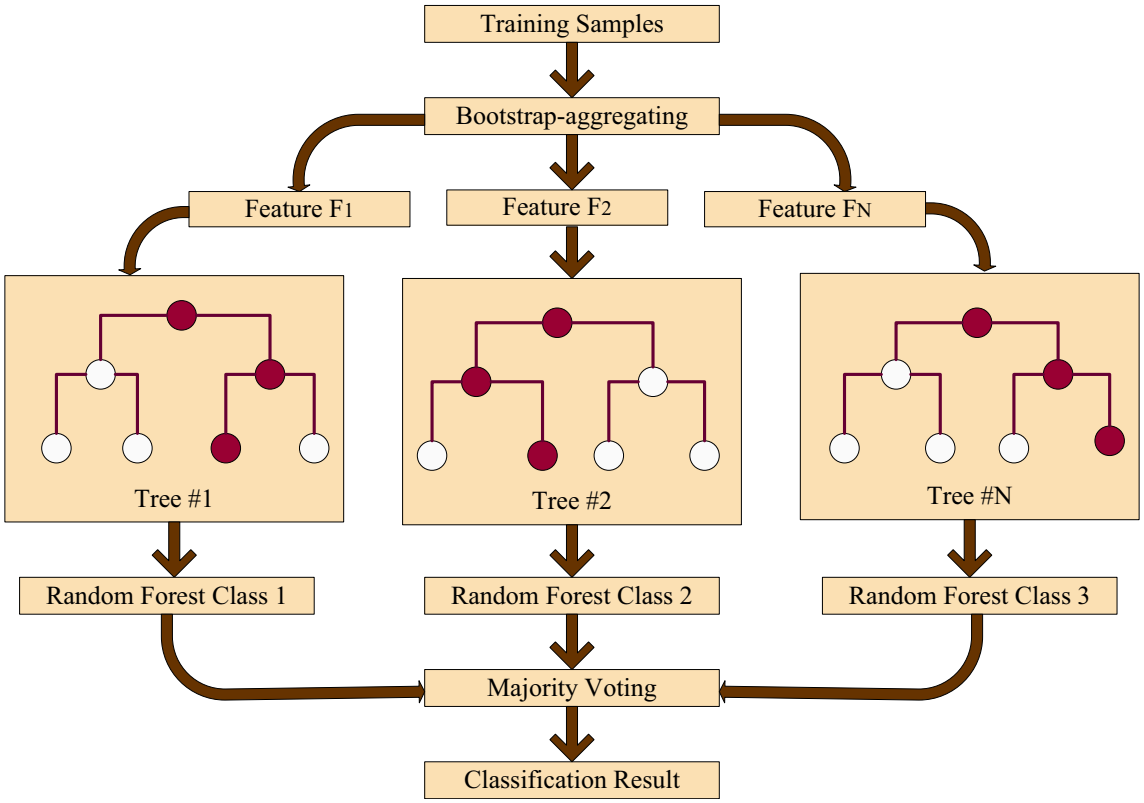


**Fig. 4** The basics of the random forest algorithm

Stage: 7 In classification, for an input U, each tree assigns a unit vote to the corresponding class. The output O(U) represents the class that the majority of the trees vote for, as denoted by (13), where $ORFT_A(U)$ is the class vote (i.e. prediction) of the Ath tree of the RF.

$$O(U) = ORFT_A(U), P = 1toC_t \tag{13}$$

In this method, the voltage signal of the solar generator is continuously analyzed by the μ-PMU. The μ-PMU then calculates the symmetrical components of the voltage. The angular sum between the zero and negative sequence components is calculated in the μ-PMU and is compared against a threshold to detect island. To obtain the threshold values needed, several scenarios are simulated such as island, faults and normal conditions and the graphs are plotted in Figs. 5, 6, 7, 8, 9 and 10. The graphs show that the angular sum between the zero and negative sequence components has different characteristics for different scenarios. The threshold value (i.e. the maximum angular sum) are different in each case. The threshold is considered as the maximum angular sum and the values are provided in Table 1. However, these thresholds cannot be determined based on few cases. Hence, as provided in Table 2, a number of scenarios has been simulated to determine the threshold. These threshold values act as the input feature for training the RF classifier. The RF classifier has been compared with other classifier models in Table 3 which shows its supremacy over other classifiers for this particular application.

### 3.4 Stages of the proposed algorithm

The proposed algorithm is illustrated in Fig. 11. The initial phase detects the occurrences, whereas the subsequent phase implements post-event measures to bolster resilience. Detailed descriptions of the sequential stages follow.

Stage 1 The μ-PMU obtains the voltage data of the solar generator bus.

Stage 2 Fortescue Transform is performed to calculate maximum angular sum, symmetrical components of the voltage signal is done and the information obtained in 10 ms i.e. 10,000 samples to calculate the angular sum between the zero and negative sequence components.

Stage 3 The maximum angular sum between the zero and negative sequence component is obtained.

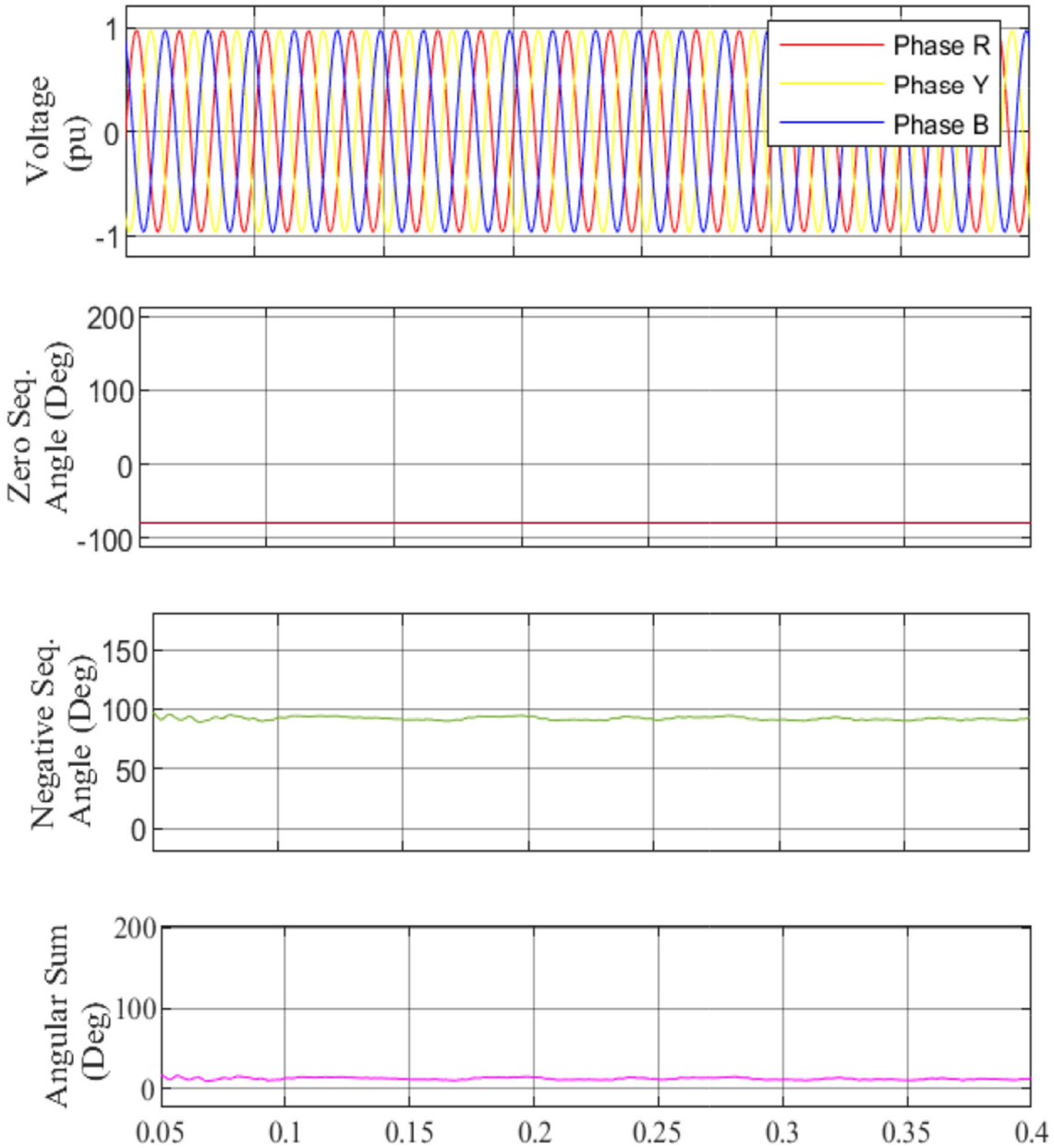


**Fig. 5** Under normal condition, the three phase voltage waveforms (represented by the R phase in red, the Y phase in yellow, and the B phase in blue) along with the angle of zero and negative phase sequences and their angular sums are illustrated (color figure online)

Stage 4 The maximum angular sum is fed to the RF classifier model for cataloguing of the events.

Stage 5 The flow goes to Stage 6 on detection of fault or island else it goes to Stage 1.

Stage 6 The detected event is shared with the nearby substations.

## 4 Performance of the algorithm

It is proposed to simulate a number of different scenarios in order to illustrate the resilience of the approach. Table 4 presents the findings for the various island situations using active power imbalance (at zero reactive power mismatch). It is obvious to see that when there is no power discrepancy at all, the algorithm operates well. This demonstrates that the algorithm does not have any NDZ. The outcomes for

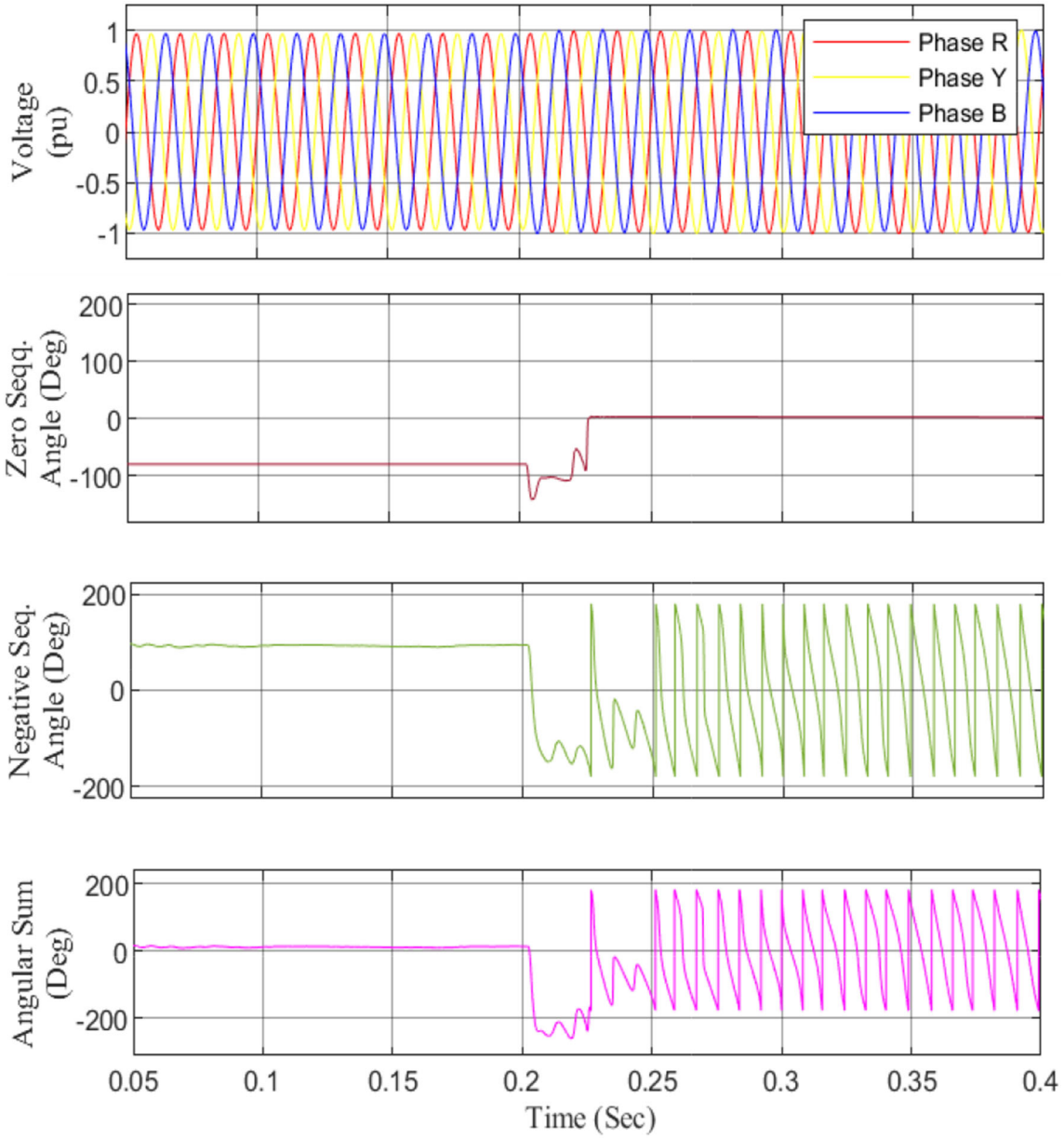


**Fig. 6** Under islanding condition, the three phase voltage waveforms (represented by the R phase in red, the Y phase in yellow, and the B phase in blue) along with the angle of zero and negative phase sequences and their angular sums are illustrated (color figure online)

the island situations for the numerous reactive power mismatches are presented in Table 5 (at zero active power mismatch). It is evident, after looking at Tables 4 and 5, that the procedure provides accurate results for every circumstance involving an island.

The results of the faults are presented in Tables 6 and 7, respectively, and are subdivided by fault inception angle (FIA) and fault resistance (FR). In order to accomplish this goal, the MG was given a number of LG, LLG, LL, and LLL faults, each of which featured a unique fault resistance and FIA. The findings demonstrate that the precision of the approach is not contingent on the fault kinds, fault resistance, or FIA. However, the method gives inaccurate results for FR above 90 Ω and FIA above 300°.

The findings of the algorithm used in various power system operations in the MG are presented in Table 8. Taking into consideration are several potential outcomes, such as the switching of a capacitor with 250 kVAR, the

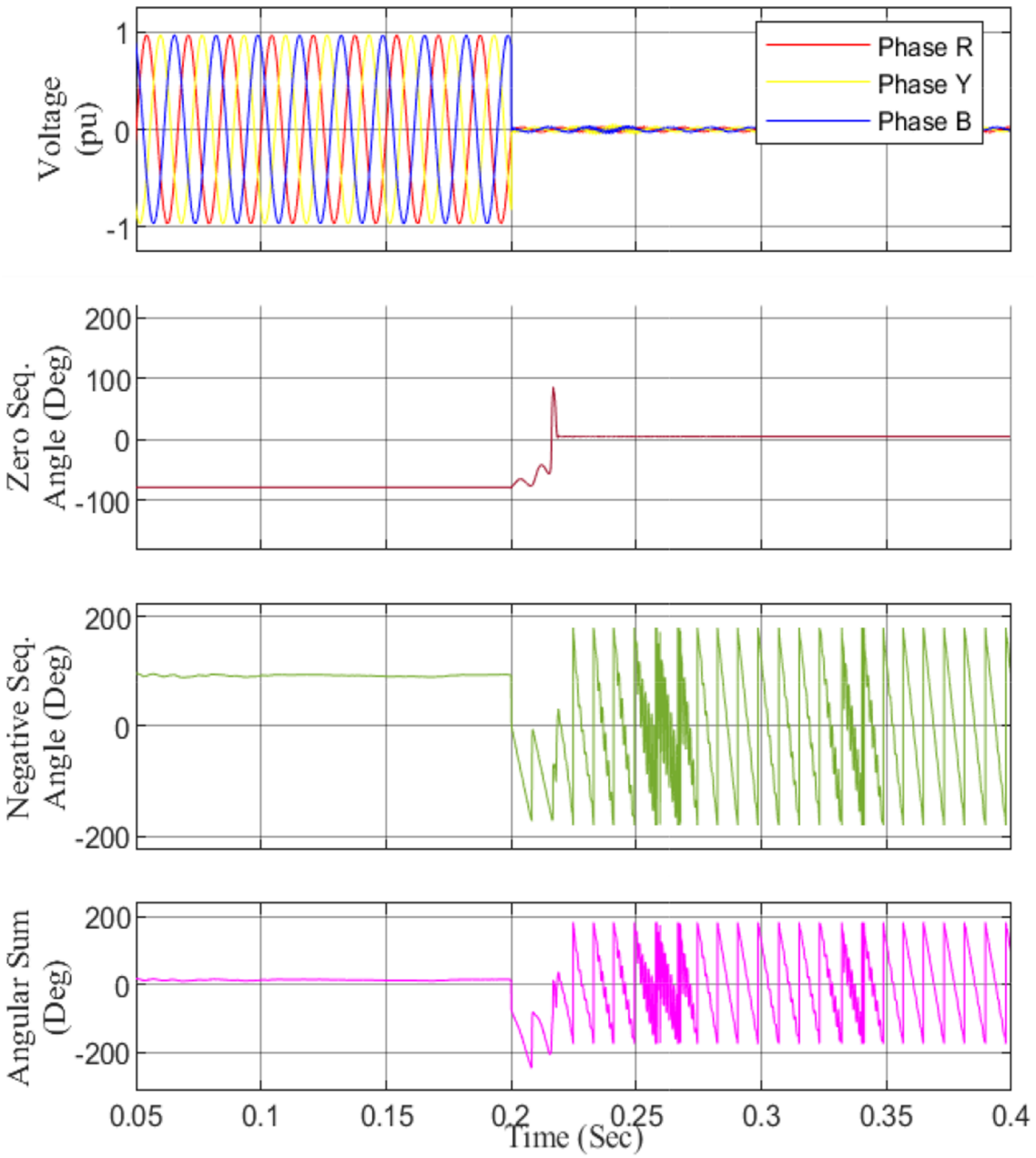


**Fig. 7** Under LLL-fault condition, the three phase voltage waveforms (represented by the R phase in red, the Y phase in yellow, and the B phase in blue) along with the angle of zero and negative phase sequences and their angular sums are illustrated (color figure online)

unmasking of a load with 200 kW, and the beginning of an induction motor at the solar generator bus. In order to validate the algorithm's effectiveness in the context of faults that arise outside of the microgrid, the algorithm is additionally validated in the context of multiple faults that arise between the different nodes. In order to demonstrate how the proposed approach is affected by measurement noise, a noise level with varying signal-to-noise ratio (SNR) was superimposed on the voltage signal, and a table of the accuracy of the method versus SNR is shown in Table 9. As the SNR is increased, it can be shown that the reliability is not much affected. This is because RF is a reliable tool for combating noise sensitivity. As a result, this follows directly from that fact with a limitation of 30 dB SNR.

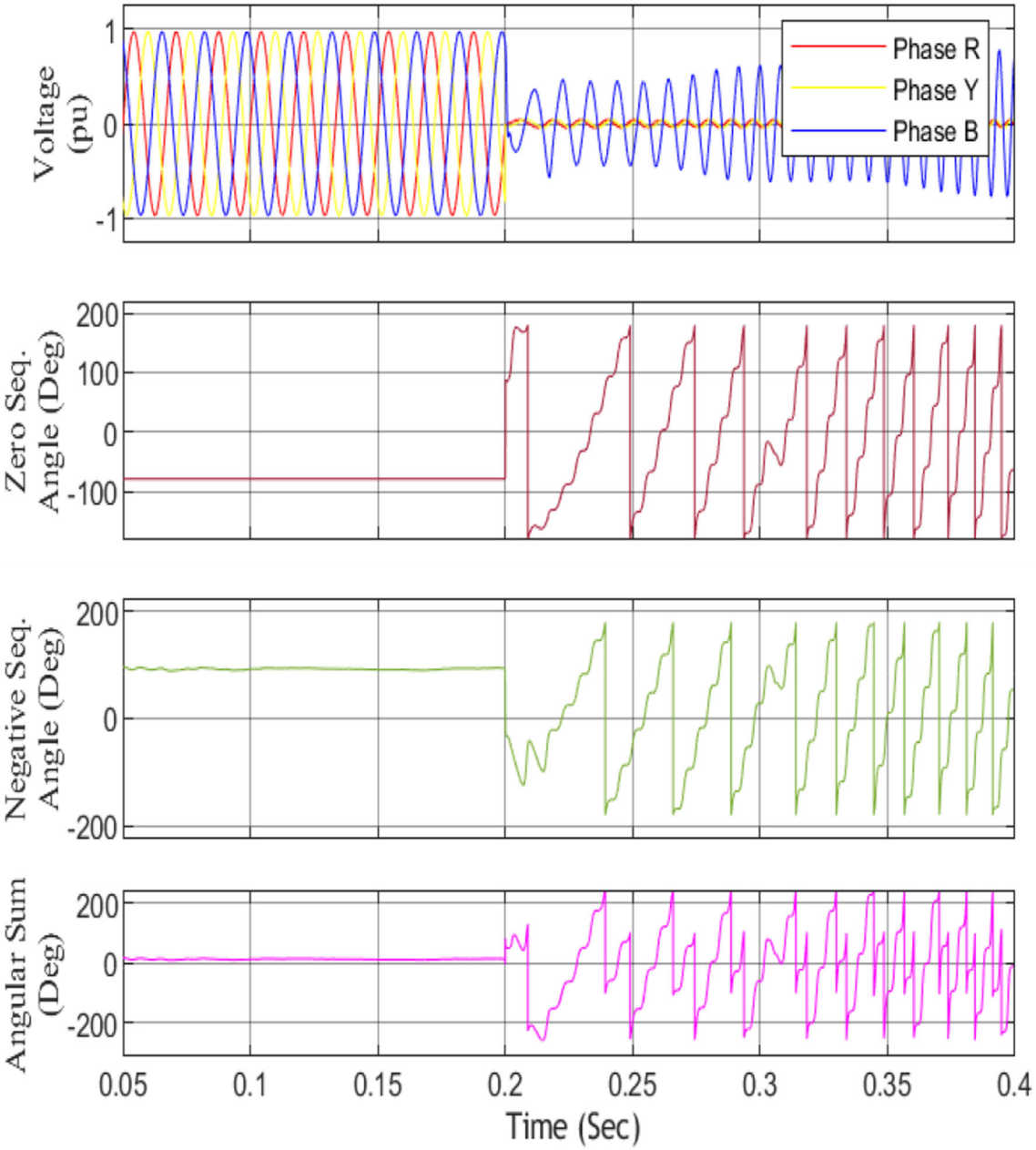


**Fig. 8** Under LLG-fault condition, the three phase voltage waveforms (represented by the R phase in red, the Y phase in yellow, and the B phase in blue) along with the angle of zero and negative phase sequences and their angular sums are illustrated (color figure online)

It is obvious to see that the algorithm generates correct results in almost every circumstance. Thus, the tables justify the robustness of the method.

### 4.1 Time of detection

**Reaction time** 10,000 samples are needed for achieving symmetrical components. Hence, the reaction time, or the time necessary to collect 8000 samples, may be determined to be 10 milliseconds (10,000 * 0.001ms).

**Program Execution time** The execution time is 5 ms as RF classifier model takes some time to give results.

**Propagation delay** Around 5 ms of lag can be attributed to voltage detection via PT, A/D conversion, etc. (Makwana and Bhalja 2017).

**Total time** In order to determine how long it takes to conduct a full island sensing, we can use the formula (1). As a result, the suggested algorithm has total detection time of around 20ms (10 + 5 + 5ms).

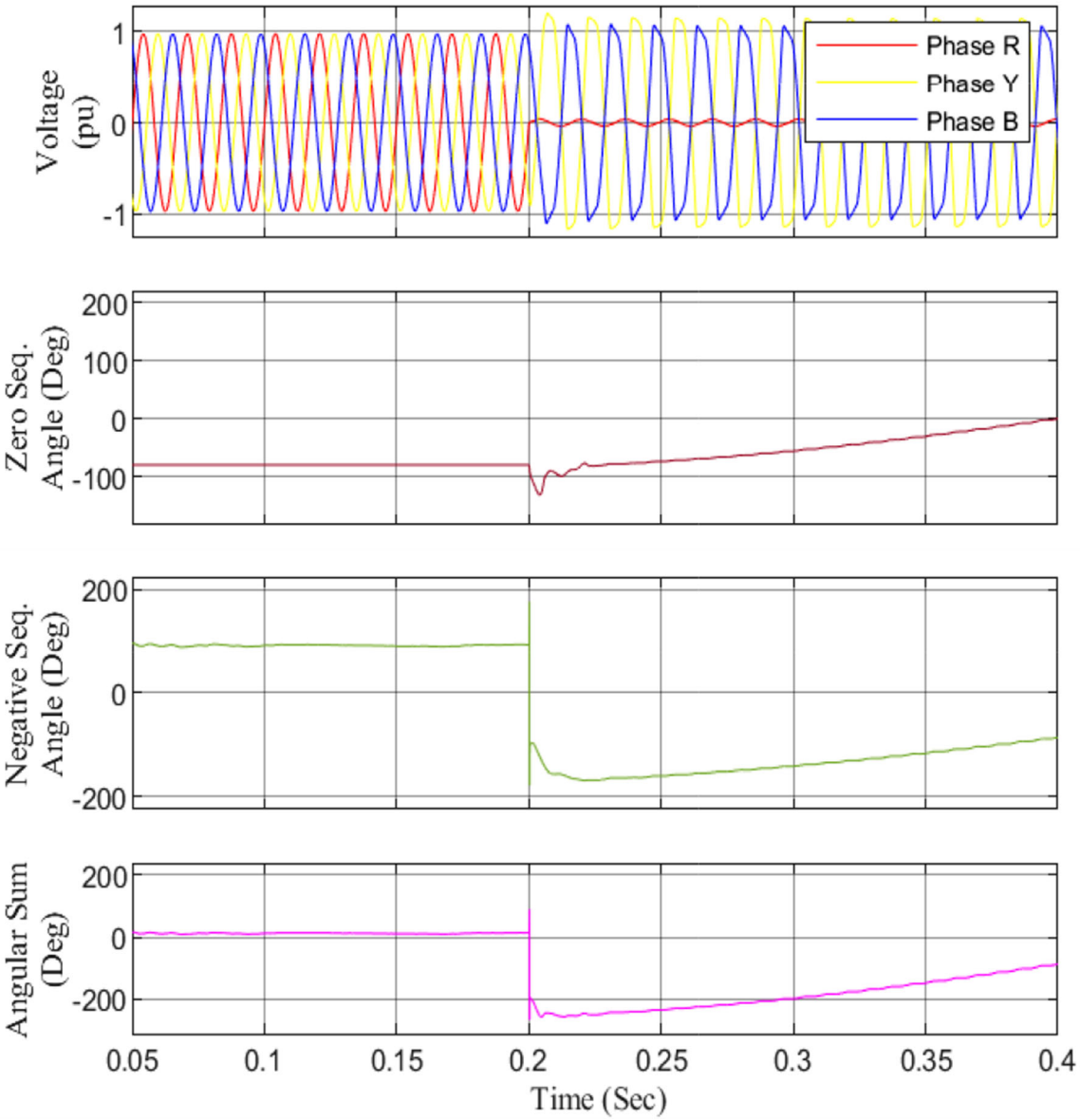


**Fig. 9** Under LG-fault condition, the three phase voltage waveforms (represented by the R phase in red, the Y phase in yellow, and the B phase in blue) along with the angle of zero and negative phase sequences and their angular sums are illustrated (color figure online)

$$[\textit{Total time}] = [\text{Program } \textit{execution time}] + [\text{Reaction } \textit{time}] + [\text{Propagation } \textit{delay}] \tag{14}$$

## 5 Assessment of the proposed technique with other approaches

The major contrast between the suggested and other detection methods mentioned in literature survey is that the present approach is programmed within μ-PMU for the purpose of unintentional islanding circumstances detection. This is the notable change. Because of this, power system engineers will have the chance to reduce the amount of time and money spent on the implementation process because all they will need to do is add a separate subroutine to the μ-PMU that has already been installed. In addition, because the process of phasor estimate is not incorporated into the algorithm, the island may be identified very fast, which is essential for increasing the grid's resilience. The method's independence on the reference phase angle as well as the reference frequency is an added benefit of using the technique. In addition to that, the method that has been proposed has the capability of fault recognizing, and also improves the situational healthiness of the grid. Some of

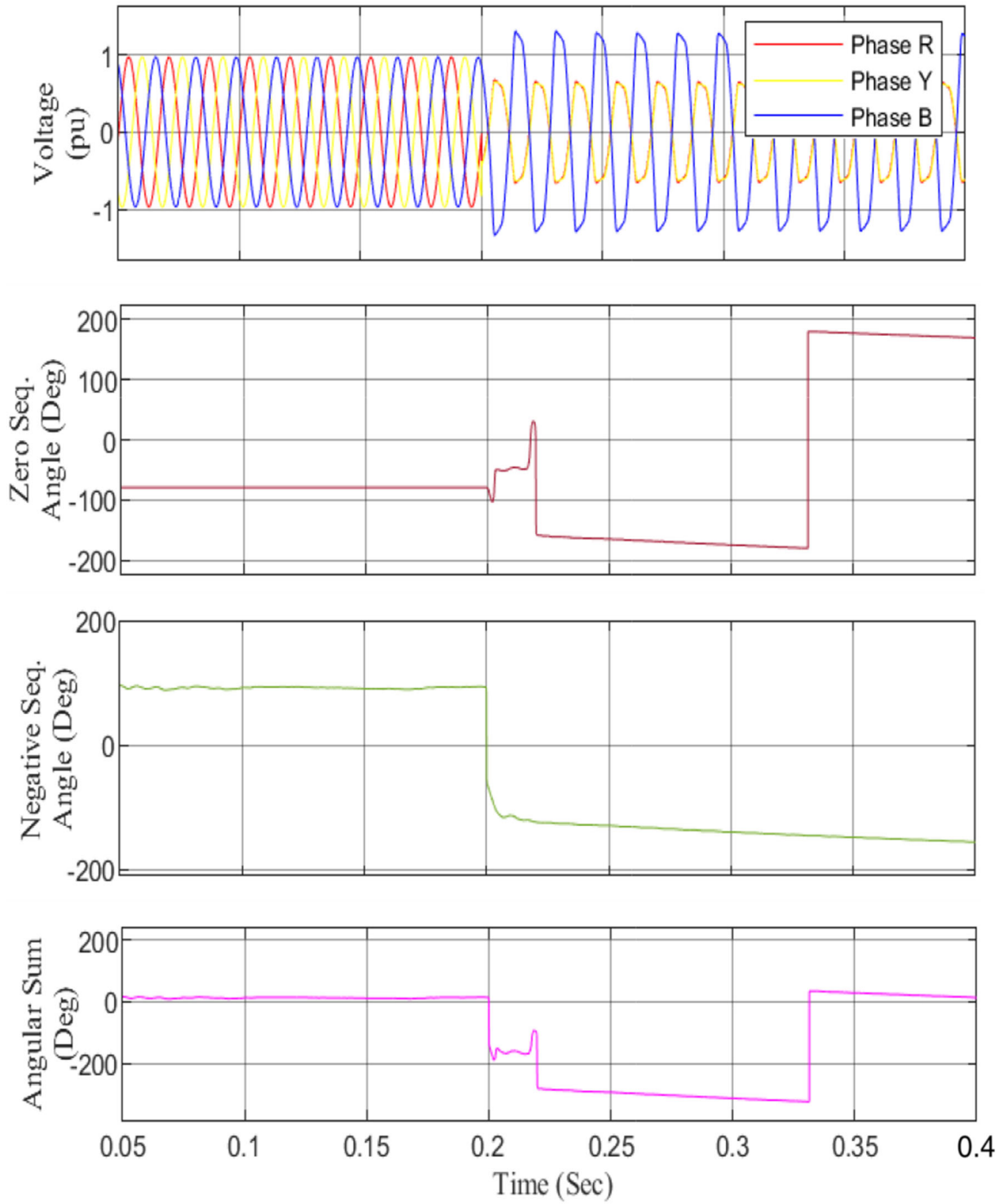


**Fig. 10** Under LL-fault condition, the three phase voltage waveforms (represented by the R phase in red, the Y phase in yellow, and the B phase in blue) along with the angle of zero and negative phase sequences and their angular sums are illustrated (color figure online)

the approaches that are currently available are replicated by employing the identical computer system using the same testing system that is described in Unit 3, and using the same types of testing scenarios that are described in Table 2. The simulation results for detection time (for approaches that do not use classifiers) and accuracy (for methods that use classifiers) are compared to the suggested approach in Tables 10 and 11 correspondingly. As

**Table 1** Values obtained from the graphs

| Case | Threshold value (deg.) |
|---|---|
| Normal | 15.71 |
| Island | 182.26 |
| LLL | 184.35 |
| LLG | 256.57 |
| LG | 89.83 |
| LL | 15.16 |

**Table 3** Classifier model and their accuracy

| Classifier model | Accuracy (%) |
|---|---|
| Artificial neural network | 95.2 |
| Support vector machine | 92.9 |
| RF | 99.3 |
| Decision tree | 81.7 |

compared to other methods, it can be noted that the proposed method takes a shorter amount of detection time while maintaining a high level of accuracy. These facets provide supporting evidence for the presented technique's superiority over alternative islanding recognition approaches.

## 6 Conclusion

As the power system continues to be subjected to exorbitant situations, the power industries have become increasingly interested in strengthening the resilience of the grid, specifically though islanding of MG. Nevertheless, the islanding under such scenarios happens inadvertently, devoid of the MG operators' previous knowledge. Therefore, this paper presents a novel and improved approach to islanding detection by implementing μ-PMU. μ-PMU based Fortescue transform with random forest algorithm is introduced for the purpose of evaluating the phase angle of sequence components. For detecting island cases, the angular sum of phase angles of a zero and negative sequence of voltage signals is utilised. The algorithm is devoid of NDZs. In order to ensure its robustness and accuracy, the proposed method undergoes simulations under a variety of conditions, including normal conditions, islanding conditions, and faults like: L-L, L-G, L-L-L, L-L-G. Furthermore, the programmed algorithm incorporates

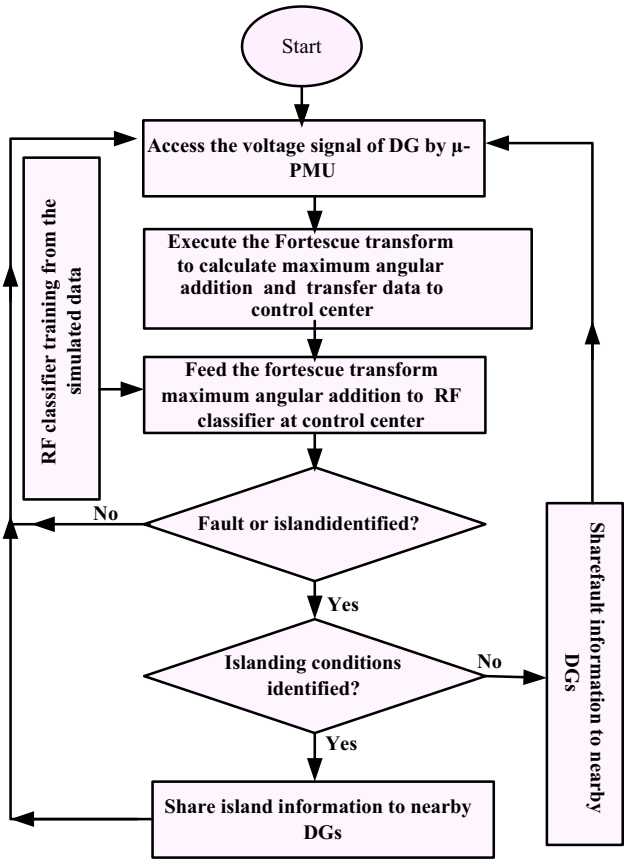


**Fig. 11** Flowchart illustrating the proposed method for intelligent control of MG and island detection using a μ-PMU

**Table 2** Situations simulated for threshold calculation

| Situations | Explanation | No. of situations |
|---|---|---|
| Island | Reactive power variation = ± 35% | 70 |
| | Active power variation = ± 35% | 70 |
| | Active and reactive power variation = ± 35% | 70 |
| Fault | Different faults (LG, LLL, LL and LLG) having fault resistance variation in range of 0Ω to 85Ω | 160 |
| Other | Switching on of loads having variation in the range of 125 kW to 225 kW kVAR | 50 |
| | Switching on of capacitor banks having variation in the range of 125 kVAR to 225 | 50 |

**Table 4** Performance of the algorithm under different power mismatch (reactive) during islanding

| % Power mismatch | Load (kW) | Classified event |
|---|---|---|
| − 80 | 50 | Island |
| − 60 | 100 | Island |
| − 40 | 150 | Island |
| − 20 | 200 | Island |
| 0 | 250 | Island |
| 20 | 300 | Island |
| 40 | 350 | Island |
| 60 | 400 | Island |
| 80 | 450 | Island |
| 100 | 500 | Island |

**Table 5** Performance of the algorithm under different power mismatch (reactive) during islanding

| Power mismatch (%) | Load (kVAR) | Classified event |
|---|---|---|
| 0 | 0 | Island |
| 50 | 50 | Island |
| 100 | 100 | Island |
| 150 | 150 | Island |
| 200 | 200 | Island |

**Table 6** Performance of the algorithm under different faults having FR

| FR (Ω) | LLG Fault | LG Fault | LLL Fault | LL Fault |
|---|---|---|---|---|
| 0 | Fault | Fault | Fault | Fault |
| 15 | Fault | Fault | Fault | Fault |
| 25 | Fault | Fault | Fault | Fault |
| 35 | Fault | Fault | Fault | Fault |
| 45 | Fault | Fault | Fault | Fault |
| 55 | Fault | Fault | Fault | Fault |
| 65 | Fault | Fault | Fault | Fault |
| 75 | Fault | Fault | Fault | Fault |
| 85 | Fault | Fault | Fault | Fault |
| 95 | Fault | Other | Fault | Fault |
| 100 | Fault | Island | Other | Island |

intelligent islanding to safeguard against the destruction of the critical load. Thus, the study's results guarantee that the proposed method for islanding detection is not only quicker, but also simpler, more cost-effective, secure, accurate, and intelligent.

**Table 7** Performance of the algorithm under different faults having FIA

| FIA (Deg) | LLG Fault | LG Fault | LLL Fault | LL Fault |
|---|---|---|---|---|
| 0 | Fault | Fault | Fault | Fault |
| 35 | Fault | Fault | Fault | Fault |
| 65 | Fault | Fault | Fault | Fault |
| 95 | Fault | Fault | Fault | Fault |
| 125 | Fault | Fault | Fault | Fault |
| 155 | Fault | Fault | Fault | Fault |
| 180 | Fault | Fault | Fault | Fault |
| 215 | Fault | Fault | Fault | Fault |
| 245 | Fault | Fault | Fault | Fault |
| 275 | Fault | Fault | Fault | Fault |
| 305 | Island | Fault | Island | Other |
| 330 | Other | Island | Fault | Fault |

**Table 8** Performance of the algorithm under different power system operations

| Operations | Classified event |
|---|---|
| Normal | Other |
| Starting an induction motor | Other |
| Unmasking of load | Other |
| Switching of capacitor | Other |
| LLL fault in middle of node 675 and 692 | Fault |
| LL fault in middle of node 632 and 633 | Fault |
| LG fault in middle of node 652 and 684 | Fault |
| LLG fault in middle of node 645 and 646 | Fault |

**Table 9** Performance of the algorithm under different noise levels

| SNR(dB) | Classified event |
|---|---|
| 10 | Island |
| 15 | Island |
| 25 | Island |
| 35 | Other |
| 45 | Fault |

Consideration may be given to a variety of prospects for future employment. Further application of the current work is possible in grids with a high proportion of electric vehicles, taking into account the rapid charging methods of electric vehicles that may introduce grid transients comparable to those caused by island detection signals. SNR limitations notwithstanding, contemporary advanced techniques including reinforcement learning, extreme learning, and spatiotemporal pattern recognition can be integrated to rectify the present method's deficiencies. Additionally,

**Table 10** Time of detection of various techniques

| Technique | Time of detection (ms) |
|---|---|
| Sandia frequency shift (Lopes and Sun 2006) | 55 |
| Sandia voltage shift (Trujillo et al. 2010) | 62 |
| Fortescue transform (Dutta et al. 2018a) | 50 |
| Slip mode frequency shift (Liu et al. 2010) | 65 |
| Present | 20 |

**Table 11** Accuracy of various techniques

| Technique | Accuracy (%) |
|---|---|
| Support vector machine and Stockwell transform | 96.41 |
| Decision tree and over-under voltage/over-under frequency (Liu et al. 2010) | 84.12/92.32 |
| Decision tree and wavelet transform (Heidari et al. 2013) | 96.31 |
| Present | 99.3 |

these approaches would be advantageous in light of the growing complexity of power grids and the magnitude of cyber threats. Additionally, future research may consider the implementation of secure methods to regulate power flow in the islanded area through the division of it into smaller islands, known as "islands of islands."

**Author contributions** All authors contributed to the study, conception and design. Material preparation, data collection and analysis were performed by AS. The first draft of the manuscript was written by AS and SD. All authors read and approved the final manuscript.

**Funding** Open access funding provided by Manipal Academy of Higher Education, Manipal. The authors declare that no funds, grants, or other support were received during the preparation of this manuscript.

**Data availability** All data included in this paper are available upon request by contact with the corresponding author.

## Declarations

**Conflict of interest** The authors declare that they have no conflict of interest.

**Open Access** This article is licensed under a Creative Commons Attribution 4.0 International License, which permits use, sharing, adaptation, distribution and reproduction in any medium or format, as long as you give appropriate credit to the original author(s) and the source, provide a link to the Creative Commons licence, and indicate if changes were made. The images or other third party material in this article are included in the article's Creative Commons licence, unless indicated otherwise in a credit line to the material. If material is not included in the article's Creative Commons licence and your intended use is not permitted by statutory regulation or exceeds the permitted use, you will need to obtain permission directly from the copyright holder. To view a copy of this licence, visit http://creativecommons.org/licenses/by/4.0/.

## References

Al-Momani MM, Al-Gharaibeh SF, Al-Dmour AS, Allaham A (2023) Islanding Detection Method based Artificial neural network. Jordan J Energy 1(1)

Arefin AA (2024) Application of the phasor measurement unit for protecting unintentional islanding of the distribution system. In: Power system protection in future smart grids. Academic Press, pp 109–132

Ashwin KV, Kosuru VSR, Sridhar S, Rajesh P (2023) A passive islanding detection technique based on susceptible power indices with zero non-detection zone using a hybrid technique. Int J Intell Syst Appl Eng 11(2):635–647

Barkat F, Cheknane A, Guerrero JM, Lashab A, Istrate M, Gavrilas M, Motas JG, Banu IV (2023) Review, analysis, and performance evaluation of the most common four active methods for islanding detection in grid-connected photovoltaic systems. Electr Power Syst Res 214:108909

Chen C, Wang J, Ton D (2017) Modernizing distribution system restoration to achieve grid resiliency against extreme weather events: an integrated solution. Proc IEEE 105(7):1267–1288

Dash PK, Padhee M, Panigrahi TK (2012) A hybrid time–frequency approach based fuzzy logic system for power island detection in grid connected distributed generation. Int J Electr Power Energy Syst 42(1):453–464

Do HT, Zhang X, Nguyen NV, Li SS, Chu TTT (2015) Passive-islanding detection method using the wavelet packet transform in grid-connected photovoltaic systems. IEEE Trans Power Electron 31(10):6955–6967

Dutta S, Sadhu PK, Jaya Bharata Reddy M, Mohanta DK (2018a) Shifting of research trends in islanding detection method-a comprehensive survey. Prot Control Mod Power Syst 3:1–20

Dutta S, Sadhu PK, Reddy MJB, Mohanta DK (2018b) Smart inadvertent islanding detection employing p-type μPMU for an active distribution network. IET Gener Transm Distrib 12(20):4615–4625

Dutta S, Sadhu PK, Reddy MJB, Mohanta DK (2020) Role of microphasor measurement unit for decision making based on enhanced situational awareness of a modern distribution system. decision making applications in modern power systems. Academic Press, Cambridge, pp 181–199

Dutta S, Sahu SK, Dutta S, Dey B (2022) Leveraging a micro synchrophasor for fault detection in a renewable based smart grid—a machine learned sustainable solution with cyber-attack

resiliency. In: e-Prime-advances in electrical engineering, electronics and energy, vol 2, p 100090
Dutta S, Sahu SK, Roy M, Dutta S (2023) A data driven fault detection approach with an ensemble classifier based smart meter in modern distribution system. Sustain Energy Grids Netw 34:101012
Farzin H, Fotuhi-Firuzabad M, Moeini-Aghtaie M (2016) Enhancing power system resilience through hierarchical outage management in multi-microgrids. IEEE Trans Smart Grid 7(6):2869–2879
Fayyad Y, Osman A (2010) Neuro-wavelet based islanding detection technique. In: 2010 IEEE electrical power & energy conference. IEEE, pp 1–6
Freitas W, Xu W, Affonso CM, Huang Z (2005) Comparative analysis between ROCOF and vector surge relays for distributed generation applications. IEEE Trans Power Delivy 20(2):1315–1324
Ghalei Monfared Zanjani M, Mazlumi K, Kamwa I (2018) Application of μPMUs for adaptive protection of overcurrent relays in microgrids. IET Gener Transm Distrib 12(18):4061–4068
Gupta P, Bhatia RS, Jain DK (2016) Active ROCOF relay for islanding detection. IEEE Trans Power Deliv 32(1):420–429
Heidari M, Seifossadat G, Razaz M (2013) Application of decision tree and discrete wavelet transform for an optimized intelligent-based islanding detection method in distributed systems with distributed generations. Renew Sustain Energy Rev 27:525–532
Karimi H, Yazdani A, Iravani R (2008) Negative-sequence current injection for fast islanding detection of a distributed resource unit. IEEE Trans Power Electron 23(1):298–307
Kumar D, Bhowmik PS (2018) Artificial neural network and phasor data-based islanding detection in smart grid. IET Gener Transm Distrib 12(21):5843–5850
Laverty DM, Best RJ, Morrow DJ (2015) Loss-of-mains protection system by application of phasor measurement unit technology with experimentally assessed threshold settings. IET Gener Transm Distrib 9(2):146–153
Lidula NWA, Rajapakse AD (2012) A pattern-recognition approach for detecting power islands using transient signals—part II: performance evaluation. IEEE Trans Power Deliv 27(3):1071–1080
Liu CC (2015) Distribution systems: reliable but not resilient? [in my view]. IEEE Power Energ Mag 13(3):93–96
Liu F, Kang Y, Zhang Y, Duan S, Lin X (2010) Improved SMS islanding detection method for grid-connected converters. IET Renew Power Gener 4(1):36–42
Liu X, Laverty DM, Best RJ, Li K, Morrow DJ, McLoone S (2015) Principal component analysis of wide-area phasor measurements for islanding detection—a geometric view. IEEE Trans Power Deliv 30(2):976–985
Liu S, Zhuang S, Xu Q, Xiao J (2016) Improved voltage shift islanding detection method for multi-inverter grid-connected photovoltaic systems. IET Gener Transm Distrib 10(13):3163–3169
Lopes LA, Sun H (2006) Performance assessment of active frequency drifting islanding detection methods. IEEE Trans Energy Convers 21(1):171–180
Makwana YM, Bhalja BR (2017) Experimental performance of an islanding detection scheme based on modal components. IEEE Trans Smart Grid 10(1):1025–1035
Manikonda SK, Gaonkar DN (2019) Comprehensive review of IDMs in DG systems. IET Smart Grid 2(1):11–24
Menon V, Nehrir MH (2007) A hybrid islanding detection technique using voltage unbalance and frequency set point. IEEE Trans Power Syst 22(1):442–448
Mohanty SR, Kishor N, Ray PK, Catalo JP (2014) Comparative study of advanced signal processing techniques for islanding detection in a hybrid distributed generation system. IEEE Trans Sustain Energy 6(1):122–131
Mohanty A, Rout B, Pradhan R (2023) A comparative studies on different islanding detection methods for distributed generation systems. Energy Sour Part A Recov Util Environ Eff 45(1):2284–2316. https://doi.org/10.1080/15567036.2023.2186544
Mumtaz F, Imran K, Abusorrah A, Bukhari SBA (2023) An extensive overview of islanding detection strategies of active distributed generations in sustainable microgrids. Sustainability 15(5):4456
Nale R, Venkatanagaraju K, Biswal S, Biswal M, Kishor N (2019) Islanding detection in distributed generation system using intrinsic time decomposition. IET Gener Transm Distrib 13(5):626–633
Niaki AM, Afsharnia S (2014) A new passive islanding detection method and its performance evaluation for multi-DG systems. Electr Power Syst Res 110:180–187
Pal D, Mallikarjuna B, Reddy RJ, Reddy MJB, Mohanta DK (2017) Synchrophasor assisted adaptive relaying methodology to prevent zone-3 mal-operation during load encroachment. IEEE Sens J 17(23):7713–7722
Raza S, Mokhlis H, Arof H, Laghari JA, Wang L (2015) Application of signal processing techniques for islanding detection of distributed generation in distribution network: a review. Energy Conv Manag 96:613–624
Reddy SVR, Premila TR, Reddy CR, Gulzar MM, Khalid M (2023) A new variational mode decomposition-based passive islanding detection strategy for hybrid distributed renewable generations. Arab J Sci Eng 48(11):15435–15443
Ropp ME, Begovic M, Rohatgi A (1999) Prevention of islanding in grid-connected photovoltaic systems. Prog Photovolt Res Appl 7(1):39–59
Shukla A, Dutta S, Sahu SK, Sadhu PK (2023) A narrative perspective of island detection methods under the lens of cyber-attack in data-driven smart grid. J Electr Syst Inform Technol 10(1):1–32
Singh S, Dutta S, Sahu SK, Sadhu PK (2021) Spectral kurtosis-based island detection technique. In: Advances in smart grid automation and Industry 4.0: select proceedings of ICETSGAI4. Springer Singapore, pp 699–706
Somalwar RS, Shinde DA, Kadwane SG (2023) Performance evaluation of voltage ripple-based passive islanding detection method for a single-phase utility-connected micro-grid system. IETE J Res 69(2):854–861
Thakur AK, Singh S, Singh SP (2023) Modal voltage decomposition-based passive method for islanding detection using variational mode decomposition in active distribution network. Electr Power Syst Res 220:109378
Trujillo CL, Velasco D, Figueres E, Garcerá G (2010) Analysis of active islanding detection methods for grid-connected microinverters for renewable energy processing. Appl Energy 87(11):3591–3605
Verma S, Dutta S, Sadhu PK, Reddy MJB, Mohanta DK (2019) Islanding detection using bi-directional energy meter in a DFIG based active distribution network. In: 2019 International conference on computer, electrical & communication engineering (ICCECE). IEEE, pp 1–4
Wang Y, Chen C, Wang J, Baldick R (2015) Research on resilience of power systems under natural disasters—a review. IEEE Trans Power Syst 31(2):1604–1613

**Publisher's Note** Springer Nature remains neutral with regard to jurisdictional claims in published maps and institutional affiliations.